Journal of Materials Chemistry B

Accepted Manuscript

ROYAL SOCIETY OF CHEMISTRY

www.rsc.org/materialsB

Journal Name

ARTICLE

The effect of PEG length on the size and guest uptake of PEG-capped MIL-88A particles

Received 00th January 20xx,
Accepted 00th January 20xx

DOI: 10.1039/x0xx00000x

www.rsc.org/

Raquel Mejia-Ariza and Jurriaan Huskens*

The surface functionalization of MOF particles with poly(ethylene glycol) (PEG) is important for their use in biomedical applications. Here, the effect of the molecular weight of a monovalent PEG-carboxylate capping ligand (MW_{PEG}) was investigated in a newly developed one-step, stoichiometric procedure that aims at functionalizing MIL-88A particles and achieving size control at the same time. The bulk of the MIL-88A particles is composed of iron(III) oxide metal clusters connected by fumaric acid as the organic ligand. The surface is functionalized with monovalent PEG-carboxylate capping ligands of different lengths. The size of the PEG-functionalized MIL-88A decreased with increasing MW_{PEG}, and nanoMOFs were obtained for long (≥ 2 kDa) PEG chains. For lower MW_{PEG}, higher concentrations of PEG were needed to obtain the maximum size effect, but the resulting sizes were still larger than for long PEGs. BET surface area, elemental analysis, zeta potential, and infrared spectroscopy measurements showed that the PEG chains were attached to the surface of the MOF particles and not in their interior. Moreover, it was demonstrated that longer chains occupy a larger surface area, and the PEG chains adopt the low-density brush conformation. Uptake and release experiments with sulforhodamine B dye (as a model drug) showed a higher and faster uptake and release for MIL-88A functionalized with PEG (20 kDa) than for native MIL-88A, which is attributed to a larger surface-to-volume ratio for the PEG-covered particles, and to the well-hydrated and accessible nature of the PEG layer in an aqueous medium. Complete release of the dye was achieved in phosphate buffered saline, the majority by counter ion exchange, and a smaller fraction in the salt form.

Introduction

Metal-organic frameworks (MOFs), or porous coordination polymers (PCPs), constitute a heavily investigated class of materials consisting of inorganic (metal ions, metal-organic or inorganic clusters) and organic building blocks (organic ligands, polymers or biomolecules).[1] MOFs have strong bonds which provide robustness and a geometrically well-defined structure.[2] MOF compositions are tuned by varying the valencies of the building blocks and by functionalizing the organic linker during or after synthesis.[3]

Recently, MOFs have been used in the field of biomedicine.[4-16] In particular for intravenous drug delivery, nanoMOFs are needed with sizes smaller than 200 nm to freely circulate through the smallest capillaries. NanoMOFs are potential nanovectors for delivering therapeutic agents to targeted areas of the body,[17] as they have large surface-to-volume ratios, high porosities, and can be functionalized easily, thus providing opportunities for controlled drug loading and release. A prerequisite for successful targeted delivery is the ability of nanoparticles to circulate in the bloodstream for a prolonged period of time.[3] To accomplish this, hydrophilic "stealth" polymers such as poly(ethylene glycol) (PEG) have been used as coating materials.[3-5]

PEG is one of the most common coating materials to shield the surface of nanomaterials (including nanoMOFs), preventing opsonic interaction and macrophage uptake, and guaranteeing prolonged blood circulation.[18,19] As reported by Gref et al.,[4] PEG has been incorporated on the surface of MIL-100 for the encapsulation and release of an antiviral drug. Moreover, nanoUiO-66 has been used as a contrast agent, functionalized with silica and PEG to enhance its biocompatibility and stability.[20] Agostoni used another approach, introducing PEG on the surface of nanoMOFs to encapsulate and release a drug for HIV treatment.[5] In this case, MIL-100(Fe) was functionalized with cyclodextrins (CD), after which the surface was decorated with adamantyl-PEG (Ad-PEG) using inclusion complexes between Ad and CD.

In particular the group of Férey has carried out pioneering work on the exploitation of biomedical applications of surface-modified nanoMOFs.[4] One of these MOFs is MIL-88A, which has been used for drug encapsulation and as a contrast agent. MIL-88A is very promising because it has a flexible framework, low toxicity, endogenous degradations products (iron and fumaric acid), is synthesized in an aqueous medium, has good biocompatibility, degradability and imaging properties, and high loading capacities compared with other systems. However, the mechanism of drug encapsulation and release

Molecular Nanofabrication group, MESA+ Institute for Nanotechnology, University of Twente, P.O. Box 217, 7500 AE Enschede, The Netherlands. Fax: +31 53489 4645; Tel: +31 53489 2995; E-mail: J.Huskens@utwente.nl

†Electronic Supplementary Information (ESI) available: XRD and BET data, particle sizes, elemental analyses, TGA data, brush density calculations, dye uptake and release data. See DOI: 10.1039/x0xx00000x

using MIL-88A, and the influence that a PEG coating exerts on these properties, has not been determined so far.

Here, we aim to control the size of MIL-88A nanoMOF particles by varying the PEG length and concentration, and to study the effect of PEG length on the loading and unloading of a dye, which functions as a model for drug encapsulation. We adapted the MIL-88A system using Fe_3O and fumaric acid as the multivalent building blocks and used different molecular weights (MW_{PEG}) of monovalent PEG carboxylates (PEG-COOH) as capping ligands, using a concept developed recently in our group.[21] In this earlier study, we showed that replacement of only a small fraction of fumarate with a stoichiometric amount of monovalent PEG-COOH (MW_{PEG} = 2 kDa) had a strong influence on the particle size. Here, the size of MIL-88A is controlled by varying the length and molecular weight of the PEG ligand and its concentration during MOF synthesis. In order to determine the packing density of the PEGs on the surface of MIL-88A, the ratio of organic to inorganic components of MIL-88A as a function of MW_{PEG} was measured and compared with theoretical calculations (assuming mushroom and brush conformations). Finally, a model drug was encapsulated using MIL-88A with and without surface functionalization with PEG-COOH to determine the drug exchange mechanism.

Results and discussion

Scheme 1 shows the concept of forming nanoMIL-88A using different PEG lengths. MIL-88A is formed by the coordination of metal clusters, Fe_3O, and organic ligands, fumaric acid, at the core and the surface is functionalized with PEG-COOH using a one-step methodology developed before.[21] Using monovalent PEG carboxylates with different lengths, the effect of polymer length and concentration on the formation of MIL-88A is evaluated.

The number of Fe_3O coordination sites and carboxylate moieties (of the bivalent fumaric acid and monovalent PEG-COOH together) was kept constant at a 1:1 stoichiometry. Previous results[21] showed that 1% of the PEG capping ligand with MW_{PEG} = 2 kDa was sufficient to achieve the maximum size decrease. However, for smaller capping ligands, higher fractions (3 or 5%) were needed to obtain the maximum size decrease, as was shown[21] for a fluor-containing small-molecule capping ligand.

Here, MIL-88A was synthesized with 1% of PEG-COOH as a function of MW_{PEG}. X-ray powder diffraction (XRD) measurements were taken for all the samples to confirm that they were crystalline, as shown in Fig. S1, ESI†. Note that the powder XRD spectra vary from sample to sample due to differences in capping ligand size and because of their flexible structure.[21,23,24] SEM images of all samples are shown in Fig. 1a-f, and the length and width were averaged and plotted as a function of PEG length, as shown in Fig. 1g,h. The size of the MIL-88A particles rapidly decreased with increasing MW_{PEG}. For MW_{PEG} ≥ 5 kDa, the size reached a plateau of ~290 nm in length and ~119 nm in width, which is the desired size for intravenous applications. Moreover, for all MW_{PEG}, the MOFs were synthesized as a function of % PEG as shown in Fig. S2, ESI†. At low MW_{PEG} (178 or 588 Da), higher fractions (3 or 5%) were needed to reach the maximum size decrease, and even then the lengths remained too large (700-1000 nm). In contrast, for MW_{PEG} ≥ 2 kDa, only 0.5% of PEG carboxylate was needed to obtain nanoMOFs. These results are in line with our earlier findings[21] for small and large molecular capping ligands, and demonstrate the importance of having steric effects induced by the polymer, next to a termination of coordination sites, to reduce the size of the particles.

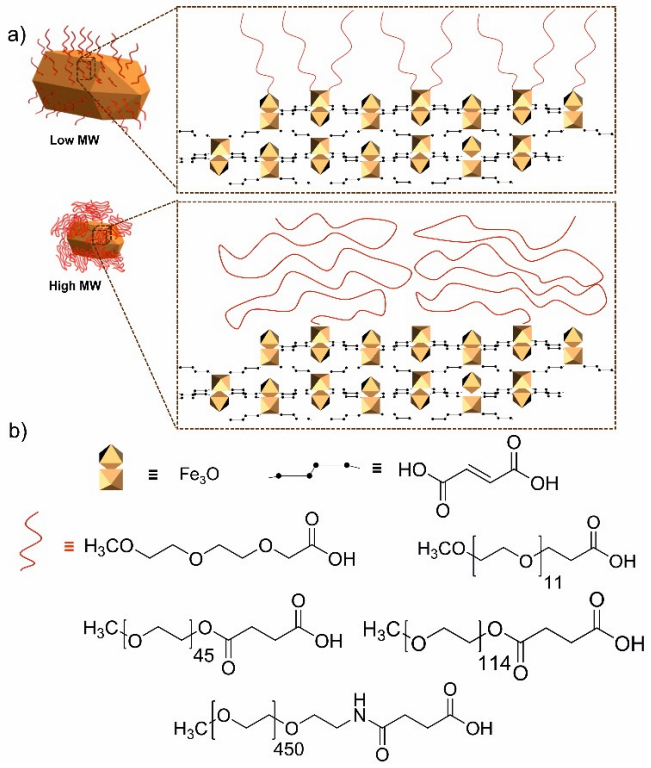

Scheme 1 a) MIL-88A synthesis: conceptual image of the introduction of different lengths of monovalent capping ligands (red) which terminate the particle surface, thereby controlling the particle size and b) Chemical structures of the building blocks used here, with the different PEG lengths corresponding to MW_{PEG} of 178, 588 Da, 2, 5 and 20 kDa.

Brunauer–Emmett–Teller (BET) surface areas were calculated from N_2 sorption isotherm measurements for four samples: non-functionalized MIL-88A, and MIL-88A functionalized with 1% of PEG-COOH with a MW_{PEG} of 178 Da, 2, and 20 kDa to study the effect of PEG length (see Fig. S3, ESI†). These results show that addition of capping ligands led to a decrease of the BET surface area, from 347 m^2/g for unfunctionalized MIL-88A to 165 m^2/g, 58.2 m^2/g and 5.8 m^2/g for the functionalized MOFs. This strong decrease is consistent with the observations made in other studies.[5,21] These results suggest that PEG is blocking the access to the pores (which is more drastic for longer PEGs) and impedes the access of gases into the MOF's interior.

Elemental analysis was performed on all samples, as shown in Table S1, ESI†. In functionalized MIL-88A, the structure is $Fe_3O(OOC\text{-}C_2H_2\text{-}COO)_3 \cdot (fumaricacid)_x \cdot Cl_z \cdot R\text{-}COO_{1-z} \cdot 3H_2O$, where R-COO is the monovalent capping ligand and free fumaric acid is occasionally adsorbed into the MOF. In order to obtain

charge neutrality, one negative charge per Fe_3O unit is needed, which is supplied either by a chloride ion or a negatively charged monovalent capping ligand (or divalent fumarate) from the synthesis mixture during preparation. The high atomic Cl/Fe ratio shown in Table S1, ESI† indicates that Cl is practically the sole counterion. More importantly, this ratio is not changing for longer PEGs. This is in agreement with the results reported previously,[21] where no fumaric acid (mono or bis-charged) or little monovalent capping ligand (only for ligands of small MW) was observed as a counterion. Moreover, little fumaric acid is bound inside the lattice, indicated by low fumaric acid fractions. At the same time, the C/Fe ratio is increasing, which is attributed to surface-attached PEG. In summary, we conclude that PEG-COOH is not incorporated as a counterion and is only attached at the surface of MIL-88A.

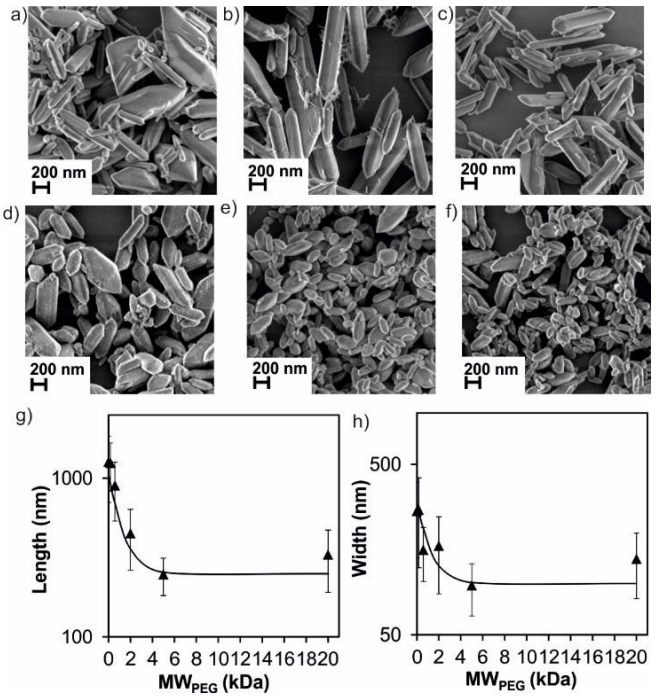

Fig. 1 SEM images of a) MIL-88A and MIL-88A functionalized with 1% PEG-COOH capping ligand as a function of MW_{PEG} for b) 178, c) 588 Da, d) 2, e) 5, and f) 20 kDa. Average values from SEM images (a-f) for: g) length and h) width, as a function of MW_{PEG}. Experimental measurements (markers) and trendlines (lines, guide to the eye).

In order to confirm that PEG is present on the MOF surface, zeta potential (ζ) and infrared (IR) spectroscopy measurements were conducted, as shown in Fig. 2 and Fig. S4, ESI†. Results from Fig. 2 show first a sharp decrease, then a gradual increase of ζ. The ζ of non-functionalized MIL-88A is positive because of an excess of free Fe sites at the surface. Probably, the native MIL-88A has not only free Fe sites, but also sites capped by fumaric acid, ending in a carboxylate. The Fe sites are in slight excess, causing the overall positive charge. After incorporation of small capping ligands (MW_{PEG} = 178 or 588 Da), these ligands block some of the surface Fe sites which leads to a decrease of about 50% of ζ. PEG itself can cause a negative zeta potential, attributed to the attraction of OH^-.[25] At higher MW_{PEG}, PEG occupies a larger surface area, resulting in the occupation of fewer Fe sites (see also the PEG packing densities discussed below). This explains the upward trend in ζ for higher MW_{PEG} as observed in Fig. 2. Moreover, IR spectra (Fig. S4, ESI†) show a C-O stretch band (which is the strongest band of PEG) for the 5 and 20 kDa samples indicating that PEG is attached on the surface of MIL-88A. These results show that longer PEGs occupy a larger surface area leading to fewer chains (in comparison with shorter chains) per unit surface area of MOF.

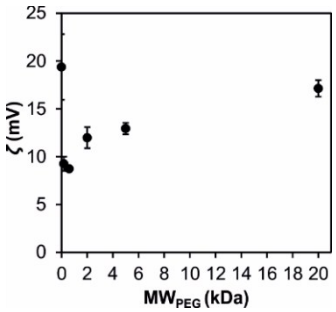

Fig. 2 Zeta potential, ζ, measurements for MIL-88A in the absence or presence of 1% of PEG-COOH capping ligand using different MW_{PEG}.

In summary, we have shown here the formation of nanoMOFs with appropriate sizes for biomedical applications, in particular for $MW_{PEG} \geq 2$ kDa. As observed previously,[21] we see a size dependence on the PEG capping ligand concentration for all MW_{PEG}. At low MW_{PEG} (≤ 588 Da), high PEG concentrations are needed to observe a large effect on the size, while at high MW_{PEG} (≥ 2 kDa), 0.5% PEG is enough to obtain nanoMOFs. At MW_{PEG} = 2, 5 and 20 kDa, higher concentrations of capping ligand do not cause a further reduction in size. This shows the importance of steric shielding from the PEG chains during the MOF synthesis and suggests that PEG is present only on the surface of MIL-88A.

After showing that the MOF size is controlled by the PEG length and concentration, understanding the packing of the PEG chains on the MOF surface as a function of PEG length is important to understand the kinetics of drug release. Thermogravimetric analysis (TGA) was used to measure the organic (m_{org}) to inorganic mass (m_{inorg}) ratio of functionalized MIL-88A as a function of PEG chain length. Two examples, for unfunctionalized MIL-88A and with 20 kDa PEG, are shown in Fig. S5a,b, ESI†. A first weight loss occurred below 100 °C, which is attributed to moisture and gas molecules adsorbed to the MIL-88A surface and inside the pores. The weight of MIL-88A remained nearly stable up to ~200°C, when fumaric acid and PEG started to decompose, until reaching 400 °C. Subsequently, the weight of MIL-88A remained unchanged until 600 °C. The remaining mass at 600 °C is m_{inorg}. For m_{org}, the loss of water (m_{water}) was calculated first and then m_{org} was calculated by subtracting m_{water} and m_{inorg} from the initial total mass. The m_{org} to m_{inorg} ratio was plotted as shown in Fig. S5c, ESI†. The m_{org}/m_{inorg} value of approx. 1.5 is in agreement with the weight ratio of fumaric acid and Fe_3O_4 corresponding to the composition of fumaric acid and Fe_3O in the bulk of MIL-88A. The results for the functionalized MOFs (Fig. S5c, ESI†) exhibit high standard deviations and the ratios are similar for functionalized and unfunctionalized MOFs, indicating that the PEG outer layer has little or no influence on the TGA results. T-tests for different sets (for selected MW_{PEG} = 0, 2 and 20 kDa)

showed no statistically significant differences between these cases, with p values higher than 0.05 (Fig. S5d, ESI†). In summary, we conclude that TGA is not sensitive enough to differentiate between different PEG lengths on the MOF surface. This indicates that the expected increase of the amount of PEG (in weight) that is attached to the MOF surface is too little to be observed by TGA.

There are several ways in which PEG may cover the surface of a material. At low surface coverage, the PEG chains exist as isolated free coils in solution, also called the "mushroom" regime. If the PEG density is increased, excluded volume interactions between chains will force extension of the PEG chains more and more, and the layer will increase in thickness. Such extended polymer conformations are called "brushes". The "brush" regime usually denotes the equilibrated state where the free energy of the crowded polymer chains in the steric layer balances the energy of creation of interface between the solution phase and the core phase.[26]

To study surface packing, Prud'homme[27] formed core-shell nanoparticles, where the core was composed of polystyrene (PS) and the surface was covered with PEG chains. They measured experimentally the PEG coverage per particle and compared these values with theoretical values using mushroom and brush regimes. Because of the large PS particle size, the surface was assumed to be flat. Here, we used the analytical approach of Prud'homme, using the same assumptions, except for the core which we take to be composed of magnetite (Fe_3O_4) only and the surface is covered with PEG. We also applied other parameters for the surface tensions using MOFs[28] and zeolites[29] instead of magnetite at the core. These calculations (not shown here) led to brush density predictions that are of the same order of magnitude as for the magnetite particles. All gave (much) higher densities than for the mushroom conformation, and the calculations for magnetite lie in between these two predictions. For both regimes, the projected diameter, ξ, i.e., the diameter of the area that a PEG chain occupies at the surface, is calculated. For the mushroom regime, the blob size is calculated using the Flory radius in a good solvent (water) as follows:

$$\xi_{mushroom} = 2 \cdot R_f = 2 \cdot a \cdot N^{3/5} \qquad \textbf{Equation 1}$$

where $\xi_{mushroom}$ is the diameter of a free polymer coil assuming no interactions between the neighboring chains, R_F denotes the Flory radius of gyration of each blob, a is the size of the individual ethylene glycol monomer (0.35 nm),[30] and N is the number of monomer repeat units. For surface packing density calculations (below), we assume a densest hexagonal packing of such PEG chains to obtain the mushroom values.

For the brush regime, the PEG spacing and brush thickness are calculated assuming an energy equilibrium of the polymer layer at the surface. Since the radius of the nanoMOF particle is much larger than the brush length, a flat plate approximation is assumed to be appropriate to estimate the projected size of a PEG brush. The approximation is based on the minimization of free energy of PEG at the interface.[26,30] The interfacial tension of the MOF functionalized with PEG suspended in water can be represented by (see ESI† for the derivation of equation 2):

$$\gamma_{eff} = (b^2/\xi^2_{brush}) \cdot \gamma_{magnetite,PEG} + (1-b^2 / \xi^2_{brush}) \cdot \gamma_{magnetite,water} \qquad \textbf{Equation 2}$$

From here on, the following equations show how to calculate the theoretical m_{org} to m_{inorg} ratios of PEG-covered MOF particles for the mushroom and brush regimes which are subsequently compared to experimental TGA measurements. After $\xi_{mushroom}$ and ξ_{brush} are calculated, the number of chains present on a particle in each regime, $\#PEG_{mushroom}$ and $\#PEG_{brush}$ ($\#PEG_i$), are first calculated using the following equation, where a_{MOF} is the particle surface area covered by PEG, as calculated from the experimental lengths and widths (see Fig. 1) using the crystal facet description as described before.[21]

$$\#PEG_i = a_{MOF} / \pi (\xi/2)^2 \qquad \textbf{Equation 3}$$

Next, the ratio m_{org} to m_{inorg} ratios for both regimes is calculated using the following equation.

$$m_{org}/m_{inorg} = (\#PEG_i \cdot MW_{PEG} + \#\text{fumaric-acid} \cdot MW_{\text{fumaric-acid}}) / \#Fe_3O_4 \cdot MW_{Fe3O4} \qquad \textbf{Equation 4}$$

where #fumaric-acid and $\#Fe_3O_4$ are calculated using the unit cells in bulk as described before.[21] $MW_{\text{fumaric-acid}}$ and MW_{Fe3O4} are the molecular weights of fumaric acid and Fe_3O_4, respectively.

Values of these parameters for PEG, magnetite, and water as shown in Table S2 (ESI†) were used to calculate the m_{org}/m_{inorg} ratios for the brush and mushroom regimes using equation 4. All theoretical values together with the experimental TGA values are plotted in Fig. 3. These results show that the brush values go significantly higher than the experimental values, even when taking the large standard deviations (Fig. S5c, ESI†) into account. The experimental values are denser than the maximum mushroom packing density, but the difference is statistically insignificant. Therefore we conclude the PEG chains are in a low-density brush conformation, and assembled in a packing in which the chains have some steric interactions with each other. In a study of MIL-88A functionalized with PEG of 5 kDa,[4] the authors concluded that the PEG chains adopted a superficial PEG `brush' sterically protecting the nanoparticles from aggregation. In summary, together with the enhanced size control effect for PEGs for the higher MWs, we assume that the PEG coverages are in a low-density brush conformation.

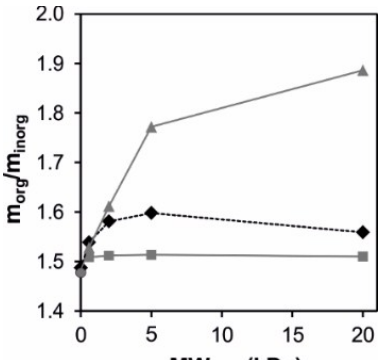

Fig. 3 m_{org}/m_{inorg} ratios of MIL-88A functionalized with 1% PEG-COOH capping ligand as a function of MW_{PEG} (kDa). Experimental (♦, black) and theoretical ratios for no PEG (●, gray), mushroom conformation (■, gray), and brush conformation (▲ gray). Trendlines are guide to the eye. For mushroom and brush regimes, it is assumed that the PEG chains are attached on a flat surface. For all the calculations, dimensions given in Fig. 1 were used.

A comparison of the packing densities of the different models is performed and compared to the density of surface coordination sites and to literature values of packing densities. Hereto, the densities of PEG (σ, mol/cm^2) were calculated from the ξ values as a function of the MW_{PEG}, as shown in Fig. S6, ESI†. When comparing the packing densities of the mushroom and brush conformations to the density of available coordination sites, we observe that the brush and mushroom packings occur always at lower densities than the available coordination sites. This implies that PEG functionalization leads to partial use of the coordination sites due to steric interactions between the PEG chains (regardless of the length of the PEG). This is in agreement with the zeta potential results discussed above. Only at low molecular weights, on the order of about 100 Da, full occupation of coordination sites can be expected without strong steric repulsion, in line with the practically complete functionalization using the small-MW fluor-containing capping ligand described before.[21]

In order to compare our model values with the literature data, we first calculated the experimental number of polymer chains (#PEGs) per surface area using the ratio of m_{org} and m_{inorg} from TGA and equation 4, and compared these values with our calculations and with values from the literature. Two series of literature values were plotted together with the mushroom, brush calculations, and experimental values as shown in Fig. S6, ESI†. The experimental values with $MW_{PEG} \geq$ 2kDa fit well between the brush and mushroom calculations and match well with the observations above that PEG chains are in a low-density brush conformation. The first literature series is a "cloud" with densities around 10^{-10} mol/cm^2 at MWs of about 10^4 Da, obtained for surface-initiated atom-transfer radical-polymerization of methyl methacrylate at different types of surfaces (flat, convex, and concave/convex) and different kinds of materials (silicate and gold).[31] These chain brushes fit between the model lines for the coordination sites and the brush regime. This indicates higher, more compressed, brush densities than expected from the thermodynamics model described above because these chains are growing from the surface starting from a high initiator density. The second data set has been obtained for PEG chains end-grafted to a gold substrate surface[32] and for PEG grafted at a PS core.[27] Here, the authors calculated the densities of these PEG chains assuming they are in the mushroom regime. However, these values are higher than our calculated mushroom values and very similar to our experimental values. All-in-all, we conclude that the PEG chains in our MOF system are in a low-density brush regime and use only part of the available coordination sites.

The encapsulation and release properties of the PEG-functionalized nanoMOFs was explored to study the effect of the PEG shell. We used the anionic sulforhodamine B as a model drug and studied its encapsulation and release using PEG-functionalized MIL-88A with different MW_{PEG}s. Because of the presence of the chloride anion in the lattice, a possible uptake and release mechanism is by counterion exchange, as shown in Scheme 2. Sulforhodamine B dye was chosen as a model drug because it is overall negatively charged and it is easy to quantify its encapsulation and release properties using fluorescence and UV/vis spectroscopy.

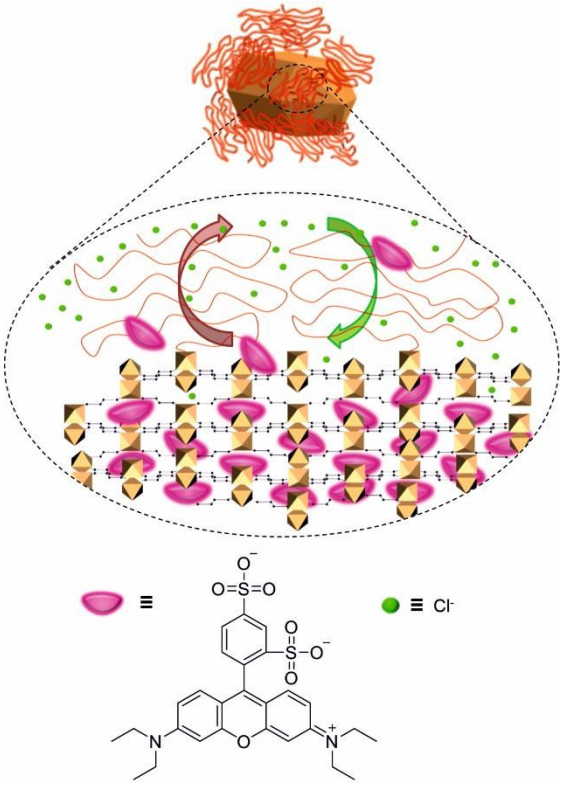

Scheme 2 Encapsulation and release of sulforhodamine B by counterion exchange.

In order to study the effect of PEG on the MOF surface, sulforhodamine B was encapsulated into two different MOFs, non-functionalized MIL-88A and MIL-88A functionalized with 1% PEG-COOH (MW_{PEG}=20 kDa; PEG20k-MIL-88A). First, the dye, in the mono Na^+ form, was encapsulated by adsorption into the porous interior of the MOF using a saturated aqueous solution, in the absence of additional salts. The loaded particles were rinsed multiple times with water, until no leaching was observed anymore. As shown in Fig. S7, ESI†, eight washings were sufficient. Subsequently, all the dye-loaded particles were washed eight times, then freeze-dried. The amount of encapsulated dye was determined by degrading

the particles with HCl for 16 h, followed by raising the pH to 7, and quantifying the dye in solution using a fluorescence calibration line (see Fig. S8, ESI†), yielding dye encapsulation results of 0.052 ± 0.007 wt% (for MIL-88A) and 0.095 ± 0.008 wt% (for PEG20k-MIL-88A). This shows that PEG20k-MIL-88A can encapsulate more dye than non-functionalized MIL-88A. A possible reason for this enhanced uptake could be entrapment of dye by the PEG layer. However, this layer is very hydrophilic and well hydrated, so it is unlikely that the PEG layer can hold the dye upon prolonged washing with water. In case the dye diffuses into the MOF interior, this diffusion is probably difficult and slow because a relatively large molecule has to move into a pore of approximately the same size. This effect has been observed for zeolites to result in preferential location of the dye in the pores that are closer to the surface.[33] In this case, the dye loading will depend on the total particle surface area, which is corresponding to the surface fraction of unit cells (SFUC).[21] Thus, the dye loading of MIL-88A and PEG20k-MIL-88A was plotted vs. SFUC, as shown in Fig. S9, ESI†. The linear trend observed here supports the idea that the loading of the dye depends on the surface to volume ratio of the particles.

Comparing these data with the literature, Horcajada et al.[4] studied the encapsulation of azidothymidine triphosphate (AZT-TP) in MIL-100 and MIL-100 coated with PEG (MIL-100-PEG, MW_{PEG} = 5 kDa). In contrast to our results, the AZT-TP encapsulation was lower in the presence of PEG (8 wt%) than without (21 wt%). This difference is attributed to an absence of an effect on the particle surface area (both particles are in the nanoregime) and the PEG layer is acting more strongly as a barrier. The higher encapsulation observed here is attributed to the 4-5 times higher pore size of MIL-100 compared to MIL-88A. Moreover, Agostoni et al.[5] have coated MIL-100 with cyclodextrin (MIL-100-CD), and encapsulated AZT-TP with a drug encapsulation efficiency of 8 wt% which is similar to the case of MIL-100-PEG. In this example, the PEG was attached using host-guest interactions between the CDs on the MOF surface and adamantyl-PEG.

The release of sulforhodamine B from the loaded particles was studied for both unmodified MIL-88A and PEG20k-MIL-88A, in the absence and presence of salt in the washing solution. To determine the release over time, we placed both samples in water and in phosphate buffer saline (PBS) (pH 7.4, 0.137 M NaCl). For each data point, half of the supernatant was removed from the dye-loaded MOF suspension and replaced by fresh water or PBS, and the amounts of sulforhodamine B in the supernatant aliquots were analysed using UV/vis calibration curves as shown in Fig. S10, ESI†. The dye release was measured for up to 5 days as shown in Fig 4a. These results show a very quick release on the first day, but the sampling was done here more frequently. When looking at the released dye per sampling point, the change in released dye is practically monotonous during the first 3 days. This indicates that equilibrium between bound and free dye is reached before a new aliquot is taken. The release is substantially higher for PBS than for water in both of samples. Moreover, PEG20k-MIL-88A releases the dye slightly faster than MIL-88A, again in agreement with the higher surface area of the former sample. After 5 days, the samples in PBS had completely released the dye, while the samples rinsed with water still contained approx. 60-75% wt% of the initially loaded dye. These results indicate that counterion exchange is the most important uptake and release mechanism. At the same time, there is a notable fraction of dye released from water, which indicates that part of the dye has also been taken up as a salt.

To study better the early release stage, possibly before reaching equilibration, we refreshed the solution more often. Thus, the experiments were repeated for a period of 6 h while refreshing the solvent every hour, as shown in Fig 4b. We observed qualitatively the same behaviour: complete release was achieved for PEG20k-MIL-88A and MIL-88A in PBS after 6 h showing that exchange of anions is needed to achieve complete dye release as compared to when only water was used. The overall release rates were somewhat faster than when the solutions were refreshed less frequently. In both solvents, the dye was released slightly faster when PEG was present on the surface, as explained by the higher surface fraction for this MOF as discussed above. Still, it is surprising to note that the PEG layer has no retarding effect on the release kinetics, this in stark contrast to the much lower BET values as discussed above. As a possible explanation, the PEG layer is well hydrated in water, providing practically unhindered access of the dye to the MOF pores from water, whereas gas adsorption in the dry state encounters a collapsed and dense PEG polymer layer that does affect its uptake. When comparing the drug release with the literature using MIL-100-PEG,[4] the AZT-TP was released much faster in the presence of PEG than without PEG, with more than 80% released after 5 h of incubation. Using MIL-100-CD,[5] the AZT-TP release in PBS was continuous and almost the same as for MIL-100. In our case, the dye was released slightly faster in the presence of PEG and the dye was completely released after 5 h.

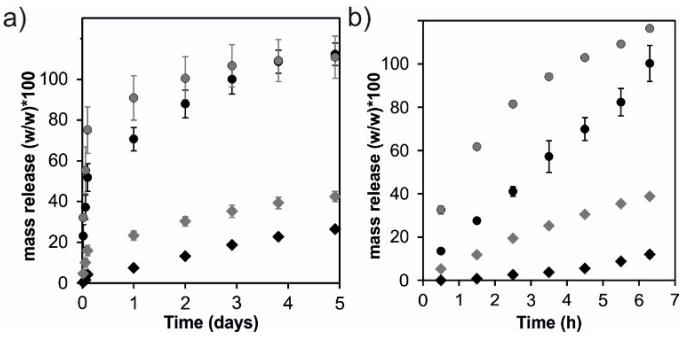

Fig. 4 Sulforhodamine B released (measured using UV/vis; see calibration lines (**Fig. S9**, ESI†.) in water (diamonds) and PBS (circles) using MIL-88A (black) and PEG20k-MIL-88A (gray), refreshing the solvent at least daily for 5 d (a), and hourly during 6.5 h (b). All experiments were carried out in triplicate (a) or duplicate (b).

Conclusions

In conclusion, we have studied the dependence of the size and properties of MIL-88A by varying the length of the capping ligand, PEG-COOH. At low MW_{PEG}, the size of MIL-88A was

found to be more sensitive to changes of the PEG length. A capping ligand with MW_{PEG} ≥ 2 kDa is needed to obtain nanoMIL-88A suitable for biomedical applications. At low MW_{PEG} (178 and 588 Da), a higher PEG concentration is needed to obtain the smallest possible particle size, but these sizes are still larger than for longer PEGs. At high MW_{PEG} (2, 5 and 20 kDa), a small PEG fraction (0.5% PEG) is sufficient to obtain nanoMOFs.

It was demonstrated that PEG chains are not incorporated in the bulk of the crystal and only attach to the surface of the MOF. Experimental organic and inorganic fractions were compared with theoretical compositions and suggest that PEG chains are present in a low-density brush conformation, slightly more densely packed than mushroom conformation. A capping ligand needs to have a small MW (about 100 Da) to occupy all coordination sites on the MOF surface; larger capping ligands lead to fractional occupation of surface sites and steric interactions between the ligands.

Encapsulation and release were demonstrated using MIL-88A and MIL-88A functionalized with PEG-COOH (20 kDa) and it was demonstrated that negatively charged molecules can be encapsulated by counterion exchange and, to a smaller extent, by diffusion into the MOF interior as a salt. Complete dye release was possible by counterion exchange using PBS. Notably, encapsulation and release was higher and faster in the presence of PEG. The higher capacity is attributed to slow diffusion within the MOF core and thus to dependence on the total surface area, which is higher for the PEG-covered MOF because of the smaller observed particle sizes. The faster release indicates that the PEG layer has no strong influence on the accessibility of the pores for guests in water, which is in stark contrast to the much lower BET values observed for gas sorption measurements in the dry state.

The improved understanding of the formation of ligand-capped MIL-88A using different PEG lengths and of the uptake and release mechanisms underlying guest encapsulation, may lead to further support for MIL-88A as a promising candidate for theranostic multifunctional nanocarriers. Control of the encapsulating and release mechanism of charged molecules allows a diverse range of applications for those MOFs, such as encapsulation of anticancer drugs (i.e. doxorubicin), antibiotics (i.e. penicillin and carbenicillin), transcription factor vectors, gases, encapsulation and delivery of small interfering RNA in humans, and DNA for the targeted delivery of genes.

Experimental

Materials

The following materials have been used as received from the supplier: Ferric chloride hexahydrate (Acros, 99%), fumaric acid (Fluka, purum), 2-[2-(2-methoxyethoxy)ethoxy]acetic (Sigma, MW 178.18), O-(2-carboxyethyl)-O'-methyl-undeca(ethylene glycol) (Sigma, MW 588.68), O-methyl-O'-succinyl-poly(ethylene glycol) (Sigma, MW~2000 and ~5000), O-[2-(3-succinylamino)ethyl]-O'-methyl-polyethylene glycol (Sigma, MW~20,000), sulforhodamine B (Sigma, dye content 75 %), ethylenediaminetetraacetic acid dipotassium salt dihydrate (EDTA) (Sigma, ≥99.0%), ethanol absolute (Merck, p.a.) and PBS (Sigma). Milli-Q water with a resistivity of 18.2 MΩ•cm at 25° C was used for the synthesis of the MOFs and for the drug encapsulation and release of sulforhodamine B.

Apparatus

For XRD experiments a D2 Phaser (Bruker) using a Cu X-ray source was used. For HRSEM a Zeiss 1550 FE-SEM was used. The particle dimensions are obtained from SEM images with ImageJ software, for each sample at least 50 particles were measured. The MIL-88A samples functionalized with 1% PEG-COOH capping ligand with different MW_{PEG} were analyzed by elemental analysis at the Mikroanalytisches Laboratorium Kolbe (Mülheim an der Ruhr, Germany), as follows: C, H were measured with a CHNOS-Analyzer from Elementar, Fe was measured after an acidic destruction with an Analyst 200 AAS from Perkin Elmer, and Cl and F were measured with a IC 883 from Metrohm. The BET measurements were performed on an Autosorb-1 from Quantachrome. The samples were degassed at 155°C for 3 h. TGA was performed using a Pyris 1 TGA Perkin Elmer on dried modified and unmodified MIL-88A under oxygen flow (20 mL/min) at a heating rate of 10 °C/min from 40-600 °C. Zeta potentials were measured on a Zetasizer NanoZS (Malvern Instrument Ltd, Malvern, United Kingdom) at 20 ˚C, with a laser wavelength of 633 nm and a scattering angle of 173˚. FT-IR analysis was performed using a Nicolet 6700 instrument (Thermo Scientific) in transmission mode. Fluorescence spectra were recorded using a Perkin Elmer LS 55 fluorescence spectrophotometer equipped with a high energy pulsed Xenon source for excitation. Emission and excitation slits were kept constant at 10 nm and scan speed of 100 nm/min using an excitation wavelength of 560 nm sulforhodamine B. UV/Vis absorption spectra were recorded using a Perkin Elmer Lambda 850 UV-Vis spectrometer. Two calibration curves of sulforhodamine in water and PBS were performed. The t-test was performed using two-tailed and two-sample t-test with unequal variance (heteroscedastic).

Synthetic procedures

The native and PEG-covered MOFs were synthesized using the procedures described previously[21] for the native MOF and the MOF using the PEG capping ligand with MW_{PEG} = 2 kDa.

Methods

Sulforhodamine B encapsulation in MIL-88A and in PEG20k-MIL-88A (MW_{PEG} = 20 kDa)

Sulforhodamine was adsorbed into the pores of MIL-88A or PEG20k-MIL-88A using a suspension of 61 or 63.8 mg of dehydrated solid and 536 or 443.4 mg of sulforhodamine B in 24.4 or 25.52 mL of water, respectively at room temperature by mixing for 16 h. The sulforhodamine-loaded particles were collected by centrifugation at 8000 rpm for 10 min and washed 8 times with water followed by freeze-drying.

In order to measure the amount of encapsulated dye, ~1.5 mg of the sulforhodamine-loaded particles was degraded under acidic conditions (~1.5 mL of 5 M aqueous HCl at 50°C overnight). Experiments were done in triplicate. Then, EDTA was added to the solution, the pH of the solution was raised to 7 and the solution was measured using fluorescence spectroscopy using a calibration curve as shown in Fig S8, ESI†.

Sulforhodamine B release in water and PBS

The release of sulforhodamine B was studied by suspending ~2 mg of non-functionalized and functionalized MIL-88A nanoparticles containing sulforhodamine B in 1 mL water or PBS (pH 7.4). These suspensions were kept by mixing for different incubation times (from 30 min to 5 d, or from 30 min to 6.5 h). At each time point, an aliquot of 0.5 mL of supernatant was recovered by centrifugation (1000 rpm/10 min) and replaced with the same volume of fresh solvent. The dye release was measured using the UV calibration curves shown in Fig S9, ESI†. Experiments were done in triplicate (series from 30 min to 5 d) or duplicate (series from 30 min to 6.5 h).

Acknowledgements

This research was supported by the Council for Chemical Sciences of the Netherlands Organization for Scientific Research (NWO-CW, Vici grant 700.58.443 to J.H.). We thank the Inorganic Materials Science group (University of Twente) for the use of the XRD equipment, Cindy Huiskes from the Inorganic Membranes group for the sorption experiments, the Materials Science and Technology of Polymers group for the TGA measurements, the Biomaterials Science and Technology group for the zeta potential measurements and Mark A. Smithers for HR-SEM imaging.

Notes and references

1 A. K. Cheetham, C. N. R. Rao, *Science* **2007**, *318*, 58-59.
2 J. L. C. Rowsell and O. M. Yaghi, *Micropor. Mesopor. Mat.* **2004**, *73*, 3-14.
3 P. Horcajada, R. Gref, T. Baati, P. K. Allan, G. Maurin, P. Couvreur, G. Férey, R. E. Morris and C. Serre, *Chem. Rev.* **2011**, *112*, 1232-1268.
4 P. Horcajada, T. Chalati, C. Serre, B. Gillet, C. Sebrie, T. Baati, J. F. Eubank, D. Heurtaux, P. Clayette, C. Kreuz, J.-S. Chang, Y. K. Hwang, V. Marsaud, P.-N. Bories, L. Cynober, S. Gil, G. Ferey, P. Couvreur and R. Gref, *Nat. Mater.* **2010**, *9*, 172-178.
5 V. Agostoni, P. Horcajada, M. Noiray, M. Malanga, A. Aykaç, L. Jicsinszky, A. Vargas-Berenguel, N. Semiramoth, S. Daoud-Mahammed, V. Nicolas, C. Martineau, F. Taulelle, J. Vigneron, A. Etcheberry, C. Serre and R. Gref, *Sci. Rep.* **2015**, *5*, 1-7.
6 W. J. Rieter, K. M. Pott, K. M. L. Taylor and W. Lin, *J. Am. Chem. Soc.* **2008**, *130*, 11584-11585.
7 K. M. L. Taylor-Pashow, J. D. Rocca, Z. Xie, S. Tran and W. Lin, *J. Am. Chem. Soc.* **2009**, *131*, 14261-14263.
8 I. Imaz, M. Rubio-Martinez, L. Garcia-Fernandez, F. Garcia, D. Ruiz-Molina, J. Hernando, V. Puntes and D. Maspoch, *Chem. Commun.* **2010**, *46*, 4737-4739.
9 J. An, S. J. Geib and N. L. Rosi, *J. Am. Chem. Soc.* **2009**, *131*, 8376-8377.
10 N. Liedana, P. Lozano, A. Galve, C. Tellez and J. Coronas, *J. Mater. Chem. B* **2014**, *2*, 1144-1151.
11 J. Zhuang, C.-H. Kuo, L.-Y. Chou, D.-Y. Liu, E. Weerapana, C.-K. Tsung, *ACS Nano* **2014**, *8*, 2812–2819.
12 H. Hintz and S. Wuttke, *Chem. Commun.* **2014**, *50*, 11472-11475.
13 V. Agostoni, R. Anand, S. Monti, S. Hall, G. Maurin, P. Horcajada, C. Serre, K. Bouchemal and R. Gref, *J. Mater. Chem. B* **2013**, *1*, 4231-4242.
14 V. Agostoni, T. Chalati, P. Horcajada, H. Willaime, R. Anand, N. Semiramoth, T. Baati, S. Hall, G. Maurin, H. Chacun, K. Bouchemal, C. Martineau, F. Taulelle, P. Couvreur, C. Rogez-Kreuz, P. Clayette, S. Monti, C. Serre and R. Gref, *Adv. Health Mater.* **2013**, *2*, 1630-1637.
15 D. Cunha, M. Ben Yahia, S. Hall, S. R. Miller, H. Chevreau, E. Elkaïm, G. Maurin, P. Horcajada and C. Serre, *Chem. Mater.* **2013**, *25*, 2767-2776.
16 S. Devautour-Vinot, C. Martineau, S. Diaby, M. Ben-Yahia, S. Miller, C. Serre, P. Horcajada, D. Cunha, F. Taulelle and G. Maurin, *J. Phys. Chem. C* **2013**, *117*, 11694-11704.
17 R. C. Huxford, J. Della Rocca and W. Lin, *Curr. Opin. Chem. Biol.* **2010**, *14*, 262-268.
18 R. Gref, M. Lück, P. Quellec, M. Marchand, E. Dellacherie, S. Harnisch, T. Blunk and R. H. Müller, *Coll. Surf. B: Biointerfaces* **2000**, *18*, 301-313.
19 D. E. Owens Iii and N. A. Peppas, *Int. J. Pharm.* **2006**, *307*, 93-102.
20 K. E. deKrafft, W. S. Boyle, L. M. Burk, O. Z. Zhou and W. Lin, *J. Mater. Chem.* **2012**, *22*, 18139-18144.
21 T. Rijnaarts, R. Mejia-Ariza, R. J. M. Egberink, W. van Roosmalen, J. Huskens, *Chem. Eur. J.* **2015**, *21*, 10296-10301.
22 S. Surble, C. Serre, C. Mellot-Draznieks, F. Millange and G. Ferey, *Chem. Commun.* **2006**, *3*, 284-286.
23 P. Horcajada, F. Salles, S. Wuttke, T. Devic, D. Heurtaux, G. Maurin, A. Vimont, M. Daturi, O. David, E. Magnier, N. Stock, Y. Filinchuk, D. Popov, C. Riekel, G. Férey and C. Serre, *J. Am. Chem. Soc.* **2011**, *133*, 17839-17847.
24 C. Tamames-Tabar, D. Cunha, E. Imbuluzqueta, F. Ragon, C. Serre, M. J. Blanco-Prieto and P. Horcajada, *J. Mater. Chem. B* **2014**, *2*, 262-271.
25 V. Jokerst, T. Lobovkina, R. N. Zare, S. S. Gambhir, *Nanomedicine* **2011**, *6*, 715-728.
26 M. Rubinstein, R.H. Colby, Polymer Physics, *Oxford University Press*, Oxford, New York, **2003**.
27 S. J. Budijono, B. Russ, W. Saad, D. H. Adamson and R. K. Prud'homme, *Coll. Surf. A* **2010**, *360*, 105-110.
28 B. Xiao, Q. Yuan, R. A. Williams, *Chem. Commun.* **2013**, *49*, 8208-8210.
29 P. Dutourni, A. Said, T. J. Daou, J. Bika, L. Limousy, *Adv. Mater. Sci. Eng.* **2015**, *2015*, 1-7.
30 C. Demaille, J. Moiroux, *J. Phys. Chem. B.* **1999**, *103*, 9903-9909.
31 Y. Tsujii, K. Ohno, S. Yamamoto, A. Goto, T. Fukuda in Surface-Initiated Polymerization I, Vol. 197 (Ed.: R. Jordan), Springer Berlin Heidelberg, **2006**, 1-45.
32 J. Abbou, A. Anne, C. Demaille, *J. Am. Chem. Soc.* **2004**, *126*, 10095-10108.
33 A. Szarpak-Jankowska, C. Burgess, L. De Cola and J. Huskens, *Chem. Eur. J.* **2013**, *19*, 14925-14930.

Different PEG length capping ligands were used to fabricated micro- and nano- MIL-88A particles. A model drug was encapsulated and released by counter-ion exchange, and its rate was dependent on the presence of PEG chains on the surface.